energy&fuels

pubs.acs.org/EF

Article

Maltene and Asphaltene Contributions to the Formation of Water-Soluble Emerging Contaminants from Photooxidation of Paving Materials

Taylor J. Glattke, Martha L. Chacón-Patiño,* Alan G. Marshall,* and Ryan P. Rodgers

Cite This: https://doi.org/10.1021/acs.energyfuels.2c02936

Read Online

ACCESS | Metrics & More | Article Recommendations | Supporting Information

ABSTRACT: Fossil fuel-derived products commonly used to pave roads, asphalt binder and coal tar pavement sealant, have been shown to readily produce highly oxidized water-soluble photoproducts that are of environmental concern. Previous work has also demonstrated that alkane-insoluble, multicore asphaltenes potentially produce water-soluble species after exposure to photoirradiation. In this work, two main solubility fractions from the asphalt binder and coal tar sealant, maltenes (alkane-soluble) and asphaltenes (alkane-insoluble), are extracted, mixed in various ratios, and photoirradiated to decouple their contributions and determine their individual roles in the generation of water-soluble photoproducts in a solar simulator microcosm. Negative-ion (−) electrospray ionization (ESI) coupled with ultrahigh-resolution Fourier transform ion cyclotron resonance mass spectrometry revealed the relative abundances and molecular compositions of the produced water-soluble species. Moreover, the amount of water-soluble organic carbon was quantified to ascertain the contributions to organic carbon production from each solubility fraction. The results revealed that maltenes, in both asphalt binder and coal tar sealant, produced abundant water-soluble species, with a highly polydisperse molecular composition and a higher dissolved organic carbon concentration compared to asphaltenes. The compositions of the water-soluble photoproducts suggest different photooxidation pathways for both materials, which produce water-solubles with contrasting molecular features. The asphalt binder produced oxidized multicore species, whereas the coal tar sealant yielded single-core oxy-polycyclic aromatic hydrocarbons.

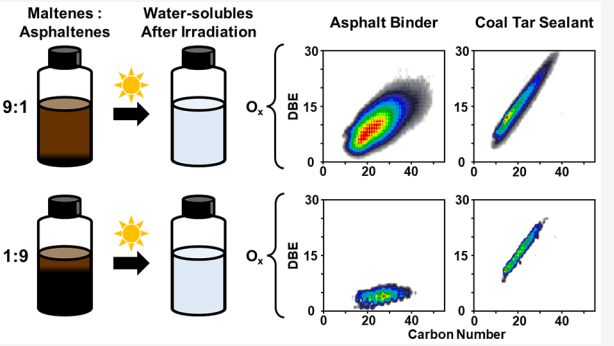

INTRODUCTION

Water-Soluble Species Formed by Photooxidation of Fossil Fuel-Derived Materials. The formation of water-soluble molecules during solar irradiation of petroleum-derived products (i.e., crude oil, asphalt binder, etc.) has been extensively studied.[1−10] Photooxidation of crude oil in a solar microcosm that mimics accidental oil spills in the ocean produces abundant oxidized species with up to 18 oxygen atoms per molecule, with much higher O/C ratios than that of the parent oils (e.g., 0.41 for weathered Macondo well oil vs ∼0.04 for the parent oil), which increases water solubility.[5,11−16]

It is critical to highlight that extra heavy fractions of crude oil (e.g., vacuum residues and asphaltenes) are extensively used in the built environment. Applications include road paving, asphalt sealers, roofing materials, waterproofing systems, and potentially material science (e.g., production of carbon fibers).[5,17−21] However, the chemistry of the emerging contaminants from fossil fuels in the built environment is not widely understood, with reports by Bowman et al.,[22] Giger and Blumer,[23] and Magi and Di Carro,[24] which suggest that they contribute to the release of carcinogenic polycyclic aromatic hydrocarbons (PAHs) into the environment as a result of the weathering. Moreover, fossil fuel products are known to be highly complex at the molecular level. For example, PetroPhase 2017 asphaltenes isolated from a Middle Eastern heavy crude oil contained ∼65,000 molecular formulas and ∼196 peaks (>6σ) at a single nominal mass at m/z 627.[25] Thus, it is important that instruments with high analytical performance, such as Fourier transform ion cyclotron resonance mass spectrometry (FT-ICR MS), are used to access the ultrahigh complexity of these samples to facilitate a better understanding of how these products behave in the built environment.

Asphalt binder is composed of the highest boiling point species that remain after high-temperature vacuum distillation; this fraction is mixed with the aggregate to pave roads.[17] In a

Received: September 1, 2022
Revised: October 5, 2022

recent work, an asphalt binder product revealed photooxidation trends similar to those of crude oil samples.[5,11,26] The produced water-soluble compounds revealed higher amounts of oxygen, with the identification of compound classes with up to 18 oxygen atoms (O_{18} class). The compositional range of the water-soluble photoproducts featured higher carbon numbers and double bond equivalents (DBE = number of rings plus double bonds to carbon) as a function of increasing the number of oxygen atoms per molecule.[5] This feature has been reported for a variety of photoirradiated oil samples, such as Athabasca bitumen asphaltenes and a low-boiling petroleum distillation cut,[11] and may suggest polymerization (addition reactions) of initially produced low-molecular-weight photoproducts as a potential pathway for forming highly oxidized water-soluble compounds with higher molecular weight.[5,11]

Analysis of coal tar sealant, a coal-based product used for protecting private driveways, parking lots, and roadways, was investigated recently.[27] The material produced highly oxidized water-soluble species, with up to 12 oxygen atoms per molecule, with increased levels of toxicity due to its initial high content of PAHs (PAH concentration = 50,000−75,000 ppm).[27,28] The high PAH concentration of coal tar sealant can be attributed to a high amount of coal tar pitch (∼15−35 wt %) contained in the sealant. In addition, coal tar sealant has been banned in various states and individual cities due to its potential negative environmental impacts, such as extensive fish kills in ponds near the application site and detrimental developmental effects on marine life.[28−33] Characterization via FT-ICR MS revealed that upon irradiation, coal tar sealant produces water-soluble oxidized hydrocarbons (up to O_{12} class) and N-containing species (up to NO_{13} class). These compounds feature DBE ranges that lie along the PAH limit, a compositional boundary for fossil fuels indicative of the presence of bare/near bare PAHs.[34,35] Thus, the results highlight the abundant production of water-soluble oxidized PAHs (oxy-PAHs) from materials routinely used in the built environment.[27]

Role of Petroleum Fractions for the Generation of Water-Soluble Contaminants in the Built Environment. Petroleum and coal are fossil fuels known to consist of two main solubility fractions: maltenes and asphaltenes. *Maltenes* are the alkane-soluble, toluene-soluble fraction of crude oil and typically exhibit low heteroatom content, low DBE, and high H/C ratios (>1.2).[36] Conversely, *asphaltenes* are the alkane-insoluble, toluene-soluble fraction, known for their high aromaticity and high concentration of heteroatoms such as O, N, S, and V.[25,37] Maltenes are generally enriched in hydrocarbons [hydrocarbon class (HC)], whereas asphaltenes contain higher proportions of heteroatomic classes (e.g., S_x, $N_xO_yS_z$, and O_x), including metal complexes such as vanadyl porphyrins ($N_4O_1V_1$ class). Asphaltenes are also considered a critical component in paving products, such as asphalt binder and coal tar sealant, as they can dramatically change the rheological properties of these materials.[38,39] For instance, research has been performed to determine how the size and content of asphaltenes in asphalt binders contribute to asphalt binder performance parameters such as the microstructure, linear viscoelastic behavior, and creep rate.[40,41] Noteworthy results demonstrated that low amounts of asphaltenes (∼5 wt %), relative to the maltene phase, result in 5.1 times higher stiffness of asphalt binder. Furthermore, the creep rate decreases with the increase in asphaltene concentrations, indicating that asphaltenes play a central role in bitumen's elasticity.[40]

Moreover, previous work has provided evidence for two asphaltene structural motifs that affect the production of water-soluble photoproducts. Multicore asphaltenes consist of multiple alkyl-substituted aromatic cores interconnected by covalent bonds. These structural motifs have been demonstrated to produce abundant oxygen-containing oil- and water-soluble compounds upon solar irradiation, which potentially occurs through photofragmentation and polymerization reactions.[11] Conversely, single-core asphaltenes, which consist of a higher-molecular-weight aromatic core with alkyl side chains, were shown to resist photofragmentation and produce little to no water-soluble species.[11] Additional work has also revealed that maltenes can be transformed into asphaltenes through crude oil photooxidation reactions conducted in solar microcosms.[42,43] These new discoveries suggest that asphaltenes are key components that contribute to the generation of potentially harmful water-soluble contaminants that persist in the environment.[44] Thus, it is important to highlight that asphalt binder contains a high mass fraction (∼17−60 wt %) of asphaltenes (relative to ∼0.5−10 wt % in crude oils)[17] and, as noted earlier, produces abundant water-soluble species upon solar irradiation.[5] However, the role of potential interactions between maltenes and asphaltenes in the production of water-soluble photoproducts from paving materials is unknown, including the effect of their mass fraction within asphalt binder/sealers. The fact that water-soluble compounds are produced from solar irradiation of both asphalt binder and coal tar sealant supports the importance of analyzing each product's solubility fractions (i.e., maltenes and asphaltenes) separately to determine how each fraction contributes to the production of potentially toxic emerging contaminants. Although asphalt's maltene and asphaltene content has been investigated for subsequent impacts on rheological properties, durability, and performance,[40,45] its implication as a source of dissolved organic carbon requires research to revisit leachability to guide the rational formulation of future environmentally friendly asphalt and related fossil carbon-derived products.

Given the known toxicity of coal tar sealant water-soluble photoproducts,[27] it is important to understand which solubility fraction disproportionally produces water-soluble, potentially toxic molecules. It is likely that maltenes and asphaltenes produce different proportions of water-soluble photoproducts given their known differences in the solubility, heteroatom content, molecular structure (content of single-core vs multicore), and nanoaggregation state.[25,36,46−49] Therefore, this work aims to investigate the individual contributions of maltenes and asphaltenes in the production of water-soluble species formed during photooxidation in a solar simulator microcosm. Given the compositional complexity of the paving materials and products, ultrahigh-resolution FT-ICR MS is used to determine the compositional differences of water-soluble photoproducts generated from the irradiation of different blends of the solubility fractions (maltenes/asphaltenes) from asphalt binder and coal tar sealant by combining maltenes and asphaltenes into blends at different ratios, submerging films of the blends spread on a glass slide in water, and irradiating them by use of a solar simulator microcosm to mimic weathering of the materials in the environment. The water-soluble photoproducts are subsequently separated from the oil-soluble counterparts and analyzed by negative-ion (−) electrospray ionization (ESI)

https://doi.org/10.1021/acs.energyfuels.2c02936
Energy Fuels XXXX, XXX, XXX−XXX

and positive-ion (+) atmospheric-pressure photoionization (APPI) FT-ICR MS. The results indicate that the maltene fraction from both road paving products are responsible for the abundant production of water-soluble species with elevated levels of dissolved organic carbon. Moreover, the compositional results suggest that water-soluble photoproducts are formed through different pathways during photooxidation, which results in potentially different molecular structures. These photooxidation pathways are the subject of future research.

EXPERIMENTAL METHODS

Asphalt Binder and Coal Tar Sealant. Asphalt binder and coal tar pavement sealant were obtained from Capital Asphalt (Tallahassee, FL, USA) and Sitelab Corporation (West Newbury, MA, USA). The samples were stored in the dark in airtight containers and used as received. The binder is rated with a performance grade of 76-22, modified with a polymer to increase the rutting resistance at high temperatures.[5,50] The coal tar sealant has a known EPA priority PAH concentration between 50,000 and 75,000 ppm, as measured by the EPA method 8270D-SIM.[51] The sealant consists of ∼15−35 wt % coal tar pitch, an emulsifying agent, water, sand, clay, and other additives.[29,30] A schematic of the experimental workflow described in the forthcoming sections is included in the Supporting Information (Figure S1).

Asphaltene Precipitation. Approximately 300 mg of asphalt binder and coal tar sealant (dried under nitrogen to remove water) was transferred to glass vials separately where *n*-heptane (nC$_7$) was added dropwise to each product to isolate the C$_7$ asphaltenes according to a modified standard ASTM method (D6560-12). Asphalt binder yielded ∼81.6 wt % C$_7$ maltenes and ∼18.4 wt % C$_7$ asphaltenes, whereas coal tar sealant contained ∼83.1 wt % C$_7$ maltenes and ∼16.9 wt % C$_7$ asphaltenes. The solubility fractions were separated by centrifugation and further cleaned by redissolution in toluene and reprecipitation in nC$_7$ assisted by sonication (Branson Ultrasonics, Danbury, CT, 22 kHz, and 130 W). The fractions were dried under N$_2$ and stored in the dark for subsequent experiments and MS analysis.

Asphaltene Extrography. Native (non-irradiated) C$_7$ asphaltenes were separated into fractions based on single-core (island) and multicore (archipelago) structural motifs by a shortened version of a previously published extrography method.[52] Native asphaltene samples from asphalt binder and coal tar sealant were dissolved in dichloromethane [high-performance liquid chromatography (HPLC)-grade J.T. Baker, Philipsburg, NJ], adsorbed onto silica gel (1% mass loading), dried under nitrogen, and sequentially Soxhlet-extracted with acetone, heptane/toluene (Hep/Tol) (1:1), and toluene/tetrahydrofuran/methanol (Tol/THF/MeOH) (1:1:0.05). The three extracts were dried under nitrogen, weighed, and stored in the dark.

Photooxidation of Maltene and Asphaltene Blends. The solubility fractions (maltene and asphaltene) from the precipitation process described above were weighed out to make up the appropriate weight % ratios (1:0, 9:1, 1:1, 1:9, and 0:1 maltenes: asphaltenes) for a total of approximately 30 mg of blended material. For example, a ratio of 9:1 would consist of ∼27 mg of maltenes and ∼3 mg of asphaltenes. To prepare films for irradiation, the blends were dissolved in dichloromethane and spread in an even layer on a clean glass slide. Thin layers of the mixture were repeatedly added and dried under nitrogen until the entire 30 mg was transferred to the glass slide in an even layer. Once fully dry (∼24 h), the slide was placed in a jacketed beaker on a glass ring [to allow for a stir bar to sit underneath the glass slide (Figure S2)]. The jacket system was connected to a water chiller maintained at 27 °C. The film was submerged in 30 mL of deionized water (HPLC-grade, J.T. Baker, Philipsburg, NJ). The prepared jacketed beaker was placed in an ATLAS Suntest CPS solar simulator (300−800 nm, 250−765 W/m^2 irradiance range, 1500 W xenon lamp)[2] and irradiated for 48 h, which is equivalent to ∼12 days of exposure in natural sunlight,[53] with continuous magnetic stirring (100 rpm). After irradiation, the water was removed from the beaker by use of a Pasteur pipet and stored in the dark at approximately 3.5 °C to prevent further oxidation. The irradiated film (oil-soluble photoproducts) was removed from the glass slide by dissolution in toluene (HPLC-grade, J.T. Baker, Philipsburg, NJ), dried under nitrogen, and stored in the dark.

Total Organic Carbon Analysis. A 10 mL aliquot of the collected water that contains water-soluble photoproducts was set aside for total organic carbon (TOC) analysis. No additional modifications were made to the water samples prior to TOC analysis so that the analyzed organics between TOC and MS analysis would be as similar as possible. The analysis was completed in triplicate and provided by Huffman Hazen Laboratory (Golden, CO). TOC concentrations were determined with the UIC/coulometrics system model 5012 by use of the Standard Methods 5310B (20th edition).[54] TOC was measured directly by acidifying and sparging the water sample to remove inorganic carbon before injection into a high-temperature (900 °C) combustion furnace. The evolved CO_2 was detected by use of a coulometric detector at a detection limit of 1 mg/L.

Precipitation of Oil-Soluble Photoproducts. The dried oil-soluble photoproducts were dissolved in 1 mL of toluene and further diluted with 40 mL of pentane (HPLC grade, J.T. Baker, Philipsburg, NJ) to precipitate alkane-insoluble compounds as described in a previous work.[42] The oxidized maltenes (alkane-soluble photoproducts) were separated from the alkane-insoluble material depleted in "occluded" maltenes (photochemically produced asphaltenes or PPA) by centrifugation (Eppendorf 5810R, 3500 rpm for 10 min at 25 °C).[55] Both fractions, photooxidized maltenes and PPA, were dried under nitrogen, weighed, and stored in the dark for subsequent MS analysis.

Characterization by FT-ICR MS. *Water-Soluble Species.* A 3 mL aliquot of the collected water that contains the water-soluble photoproducts was completely dried under nitrogen and redissolved in methanol (HPLC-grade J.T. Baker, Philipsburg, NJ) to a final concentration of 250 μg/mL for analysis using by use of a negative ion (−) ESI system coupled to a custom-built 21 T FT-ICR mass spectrometer.[56] (−) ESI is the preferred ionization method to analyze water-soluble samples to target polar and acidic species commonly contained in water-soluble fractions.[11,57] The samples were directly infused into the mass spectrometer via a heated metal capillary by use of (−) microelectrospray ionization at a flow rate of 0.5 μL/min. Approximately 1.0×10^6 ion charges were externally accumulated in a Velos Pro linear ion trap (Thermo Scientific, San Jose, CA) and then transferred to a dynamically harmonized ICR cell operated with a trapping potential of 6 V.[56,58] A Predator data station assisted with data collection, with the coaddition of 100 time-domain transients (3.1 s detection period). Custom Predator and PetroOrg© software assisted with data collection, Fourier transformation, mass spectral calibration, molecular formula assignment, and data visualization.[59,60]

Oil-Soluble Species. Stock solutions of unirradiated C$_7$ maltenes and C$_7$ asphaltenes, the asphaltene extrography fractions, and the oil-soluble photoproducts from the irradiated blends (oxidized maltenes and PPA) were diluted in toluene to a final concentration of 100 μg/mL for analysis with a (+) APPI source coupled with a custom-built 21 T FT-ICR mass spectrometer. (+) APPI is the preferred ionization method to analyze oil-soluble samples to target nonpolar and aromatic species typically contained in oil-soluble fractions.[5,11] The samples were directly infused at 50 μL/min into an Ion Max APPI source (Thermo Fisher Scientific, San Jose, CA) at a vaporizer temperature of 320 °C. N$_2$ was used as a sheath gas (15 mL/min) and auxiliary gas (10 mL/min) during ionization. Gas-phase neutrals were photoionized with 10.2 eV photons from an ultraviolet krypton lamp (Syagen Technology Inc., Tustin, CA, USA). Positive ions were transferred into the mass spectrometer via a heated metal capillary (∼350 °C) and analyzed with a custom-built 21 T FT-ICR MS. Custom Predator and PetroOrg software assisted with data collection, Fourier transformation, phasing, mass spectral calibration, molecular formula assignment, and data visualization.[59,61,62]

https://doi.org/10.1021/acs.energyfuels.2c02936
Energy Fuels XXXX, XXX, XXX−XXX

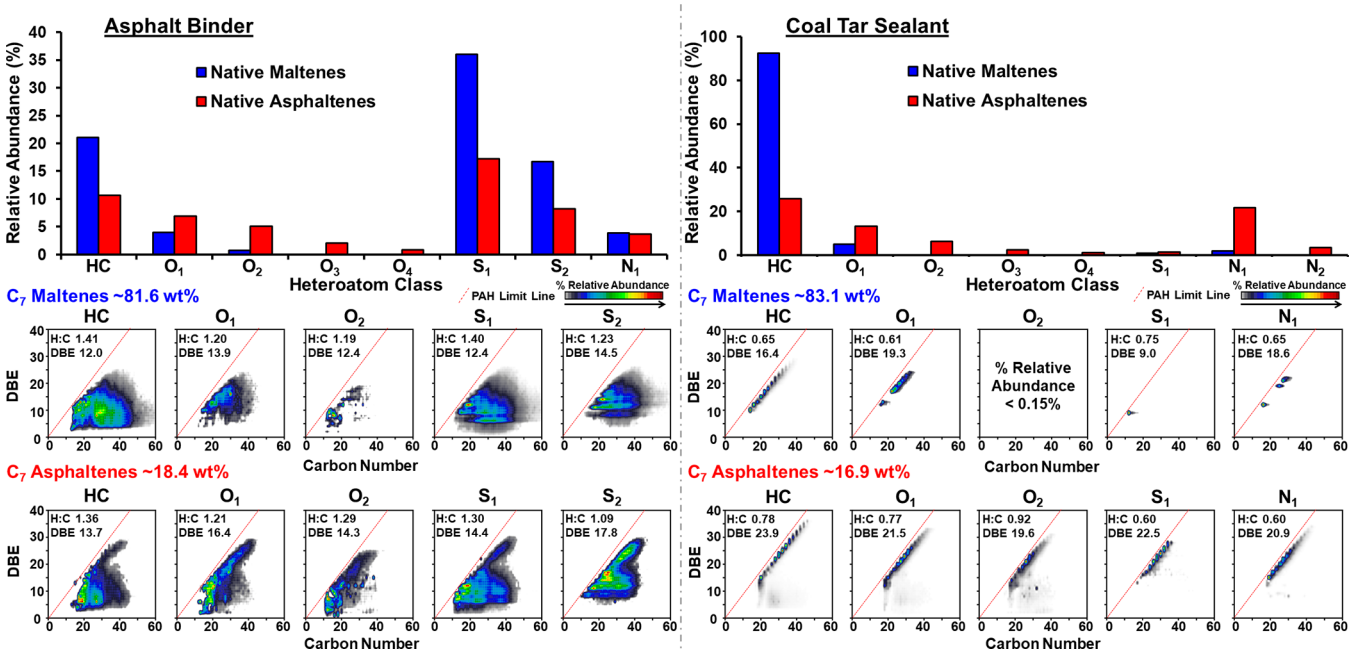

Figure 1. Heteroatom class distribution (top panels) and isoabundance color-contoured plots of DBE vs carbon number (bottom panels) derived from (+) APPI 21 T FT-ICR MS for the most abundant heteroatom classes from the analysis of asphalt binder (left) and coal tar sealant (right) solubility fractions: maltenes (blue) and asphaltenes (red).

RESULTS AND DISCUSSION

Molecular Compositions of Native Solubility Fractions. To gain insights into the molecular features of the starting materials and their possible role in the chemistry of the water-soluble photoproducts from the blends, the unirradiated solubility fractions (maltenes and asphaltenes) from asphalt binder and coal tar sealant were analyzed by direct infusion (+) APPI FT-ICR MS. The thousands of peaks detected in the mass spectra were calibrated with homologous Kendrick series,[61,63] and each was assigned a unique molecular formula ($C_cH_hN_nO_oS_s$). Compounds with equal DBE and heteroatom content but differing carbon numbers belong to the same homologous series. Simply, members of the same homologous class series feature the same DBE but have different numbers of CH_2 units (alkylation degree). Molecular formulas are sorted according to the heteroatom content; for example, all formulas with only carbon and hydrogen atoms comprise the HC class; whereas species with carbon, hydrogen, and one oxygen atom make up the O_1 class. Assignment of molecular formulas enables calculation of DBE, which represents a measure of each compound's aromaticity. MS analysis revealed distinct molecular and compositional differences between the solubility fractions of asphalt binder and coal tar sealant. Figure 1 displays the heteroatom content (top panel) and DBE versus carbon number plots (bottom panel) for the most abundant heteroatom classes detected in asphalt binder (left) and coal tar sealant (right) solubility fractions (maltenes in blue and asphaltenes in red). Abundance-weighted H/C ratios and DBE values are included in the upper left corners of the plots to facilitate sample comparison. The asphalt binder native asphaltenes contain more oxygen atoms (up to O_4) than the native maltenes (up to O_2), which is consistent with the reported higher heteroatom content for asphaltene species.[64] The asphalt binder maltenes follow typical trends for alkane-soluble compounds; this fraction contains abundant nonpolar species (HC class) and sulfur-containing classes (S_1 class), which account for more than 60% of the relative abundance.[65,66] Moreover, the maltenes and asphaltenes feature different compositional ranges. The asphaltenes extend to relatively higher DBE values (DBE ~30) and a "bimodal" compositional range that features a distribution of compounds clustered along the PAH limit line (red dashed line in each plot). The PAH limit is a compositional boundary for naturally occurring fossil fuel compounds and defines that the DBE value of planar molecules should not exceed ~90% of its carbon content. DBE values above this limit indicate the presence of fullerene-type compounds, which are not naturally abundant in fossil fuels.[34] The compositional range along the PAH limit suggests the presence of highly condensed, aromatic species within the asphaltene fraction. This finding is not surprising considering that asphaltenes are insoluble and precipitate in alkane solvents due to their higher aromaticity and higher heteroatom content. These molecular features promote strong nanoaggregation, with direct implications for asphalt binder rheological properties[40,67] and the photo-transformation of these species in the built environment. We hypothesize that species with strong aggregation trends tend to remain stable during irradiation, similar to their noted survival upon advanced hydroconversion processes.[68]

The solubility fractions from coal tar sealant show markedly different trends of heteroatom content and composition. The coal tar sealant native maltenes are rich in HC species (~92% RA) and depleted in O_1, N_1, and S_1 classes (<7% RA). This behavior is expected because previous characterization of coal tar sealant revealed a molecular composition dominated by near-bare PAHs, which are known to ionize efficiently in APPI MS.[27] The native asphaltenes contain species with higher numbers of oxygen atoms (up to O_4) and higher amounts of nitrogen-containing species (up to N_2), following the expected trend of asphaltenic compounds featuring higher amounts of heteroatom-containing molecules than that in maltenes. Compositionally, asphaltenes from coal tar sealant reveal

https://doi.org/10.1021/acs.energyfuels.2c02936
Energy Fuels XXXX, XXX, XXX−XXX

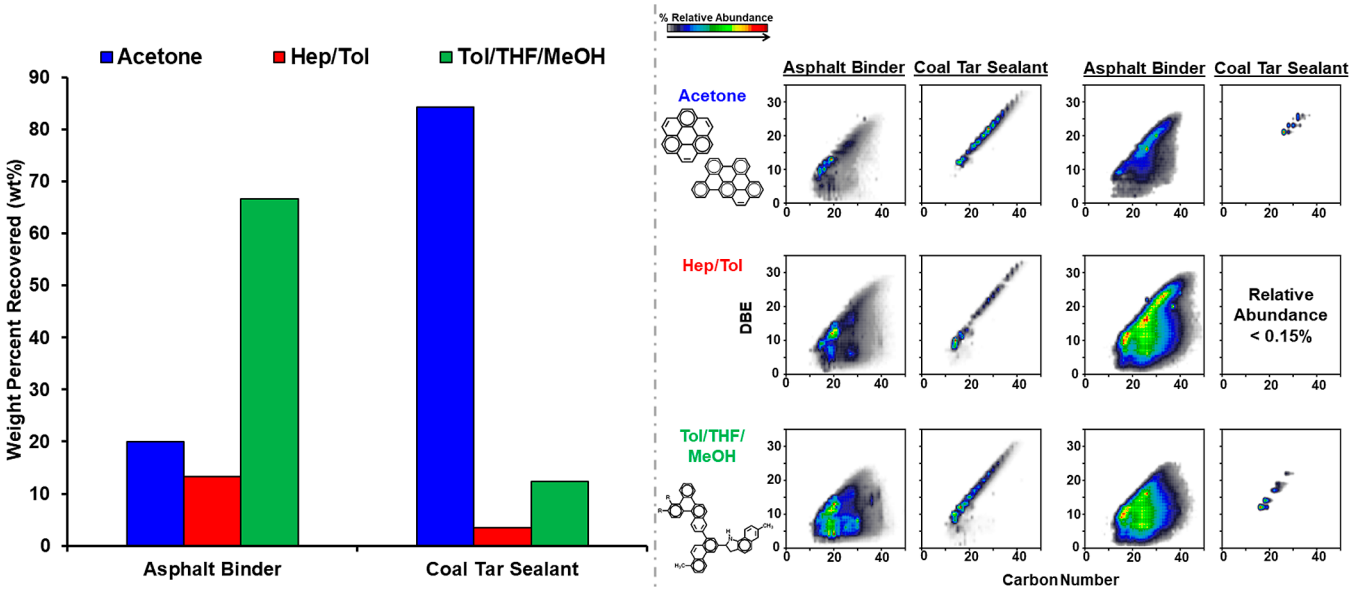

Figure 2. Weight percent recovery (left) of asphaltene extrography fractions, acetone (blue), Hep/Tol (red), and Tol/THF/MeOH (green), with combined compositional ranges (right) for the HC-, O-, and N-containing classes and S-containing classes for asphalt binder and coal tar sealant asphaltenes.

higher DBE values (AW DBE ~21.7) than the maltenes (AW DBE ~15.8). The compositional ranges of both solubility fractions from coal tar sealant lie along the PAH limit (red dashed line) and contain short homologous series (species with equal DBE but varying degrees of carbon number), which highlights the high content of alkyl-depleted (near bare) PAHs or bare PAH species.[34,69] It is important to note the similarity between the compositional ranges of coal tar sealant maltenes and asphaltenes despite the differences in their solubility behavior, which has been also reported for Illinois coal.[70] The insolubility of asphaltenes in alkane solvents can be attributed to their much higher content of heteroatoms and polarizable functionalities, which likely promotes multiple intermolecular interactions, including hydrogen bonding, which increases both molecular and nanoaggregate insolubility.[70,71]

Comparison of the compositional ranges between the asphalt binder and the coal tar sealant reveals differences consistent with trends previously noted for petroleum-derived and coal tar-derived products.[27] These include petroleum-derived products (asphalt binder and distillation cuts) that occupy a wider carbon number range (up to carbon number 60, with up to ~57 members per homologous series) than coal tar-derived compounds (up to carbon number 45 and only ~10 members per homologous series). Thus, the petroleum species studied here are highly alkyl-substituted. Furthermore, it is important to highlight the contribution of each solubility fraction to the overall content of the asphalt binder and coal tar sealant. Precipitation with heptane revealed that both products are composed of similar amounts of maltenes and asphaltenes: asphalt binder contains approximately 81.6 wt % maltenes and 18.4 wt % asphaltenes and the coal tar sealant contains approximately 83.1 wt % maltenes and 16.9 wt % asphaltenes. Because both materials are known to produce abundant water-soluble photoproducts after exposure to photooxidation,[5,27] it is important to understand the individual contributions of each solubility fraction and whether molecular structure and compositional features play a role in the formation of water-soluble species. The large differences in the compositional range and heteroatom content of the maltenes and asphaltenes suggest that upon photooxidation, both solubility fractions will likely produce different types (i.e., in terms of the compound class and/or aromaticity) and abundances of oil- and water-soluble photoproducts.

Because different asphaltene structures have been demonstrated to contribute differently to the production of water-soluble species,[11] it is also important to understand the dominant structural motifs for each product. For this purpose, asphaltene extrography was performed for C_7 asphaltenes precipitated from both asphalt binder and coal tar sealant to isolate and "quantify" fractions enriched in single-core or multicore structures. A previously reported shortened asphaltene extrography separation involves the adsorption of asphaltenes onto silica gel for subsequent extraction.[52] The asphaltene/SiO_2 mixture is dried down and extracted with acetone, enabling the separation of highly aromatic compounds with predominant dipolar intermolecular interactions with the silica gel.[52] The remaining silica and asphaltene mixture is redried and extracted with Hep/Tol to isolate remnant alkyl aromatics.[52] The mixture is finally extracted with Tol/THF/MeOH, with the ability to disrupt hydrogen bonds, thereby facilitating the liberation of abundant O- and N-containing multicore compounds from the silica gel.[52] The gravimetric yields for the extrography separation are displayed in Figure 2, left panel. Nearly 67 wt % of asphaltenes from asphalt binder was extracted in the Tol/THF/MeOH fraction, suggesting that the dominant structural motif is multicore. Conversely, approximately 84 wt % asphaltenes from the coal tar sealant were eluted in the acetone fraction, indicating that they are single-core species dominant. Figure 2, right panel, presents the combined compositional range for HC and O-/N-containing compounds (species with no sulfur atoms, leftmost plots) and all the compositions with S atoms (rightmost plots). The extrography results, along with the compositional information presented in Figure 1, allow for hypotheses about which blends are more likely to produce water-soluble species. A previous work suggested that water-soluble photo-

https://doi.org/10.1021/acs.energyfuels.2c02936
Energy Fuels XXXX, XXX, XXX−XXX

products are readily produced from multicore asphaltenes (Tol/THF/MeOH fraction), whereas single-core asphaltenes (acetone fraction) feature limited production of water-soluble emerging contaminants.[11] Thus, it is possible that the asphaltene dominant blends (1:9 and 0:1) from the asphalt binder, which are abundant in multicore asphaltenes, will produce highly oxidized water-soluble species, whereas the same blend ratios from the coal tar sealant will leach little to no heavily oxidized species. The molecular and compositional results from the unweathered maltenes and asphaltenes provide a basis for these hypotheses regarding the expected photoproducts. Thus, to test these hypotheses, the forthcoming discussion will focus on the results obtained for the photooxidized blends of asphalt binder and coal tar sealant.

Compositional Trends for the Oil-Soluble Photoproducts from Blends of Solubility Fractions from Asphalt Binder and Coal Tar Sealant. After the irradiation of the blends, the oil-soluble photoproducts were recovered and separated through precipitation with pentane into oxidized maltenes and PPA and then analyzed by (+) APPI FT-ICR MS. The weight percentages of recovered oxidized maltenes and PPA after precipitation with pentane are included in Table S1. The heteroatom class relative abundances are presented in Figure S3 and follow expected trends, with increased oxygen content after exposure to solar irradiation.[42] Generally, the asphalt binder oil-soluble photoproducts (Figure S3, left panel) present high abundances of oxygen- and sulfur-containing species; the PPA fractions (bottom left panel) reveal classes with higher oxygen content (up to O_6 and SO_5) than that of the oxidized maltenes (up to O_3 and SO_3). Regarding coal tar sealant, its oil-soluble photoproducts (Figure S3, right panel) are abundant in hydrocarbon-, oxygen-, and nitrogen-containing species, and as expected, the PPA fractions (bottom right panel) feature heteroatom classes with more oxygen atoms (up to O_6 and NO_4) than that of the photooxidized maltenes (up to O_3 and NO_2). These results are consistent with the much higher heteroatom content usually observed for alkane-insolubles.[25,37,42] Furthermore, Figures S4 and S5 display the compositional ranges for the oil-soluble photoproducts (after irradiation, oxidized maltenes and PPA) for asphalt binder and coal tar sealant. Figure S5 displays the compositions of the asphalt binder oxidized maltenes, which reveal a more extended carbon number range (up to ∼50 carbon atoms per molecule) than that of their PPA counterparts (only up to carbon number ∼40). Compositions for asphalt binder PPA lie close to the PAH limit line, which has been seen for PPA fractions in crude oil.[42] Furthermore, the compositional results highlight a bimodal distribution: the region close to the PAH limit emerges and becomes prevalent as a function of increased asphaltene content in the blends.

Figure S5 displays the compositions for the oil-soluble photoproducts from coal tar sealant. Both oxidized maltenes and PPA occupy similar compositional ranges (along the PAH limit line) as expected because coal tar sealant is heavily abundant in PAHs. The main difference lies in DBE values, with PPA fractions occupying higher DBE values (up to DBE 35) than the oxidized maltenes (DBE ∼25). The compositional trends for the *oil-soluble* photoproducts provide evidence for the photooxidation of both types of fossil fuel-derived products. However, it is crucial that we understand the individual contributions of the solubility fractions to the formation of water-soluble species that are leached upon photoirradiation from the blends. We hypothesize that this knowledge could guide the optimal formulation of environmentally friendly paving materials. Thus, the remainder of this paper will focus on the molecular composition and organic carbon concentration of the *water-soluble* photoproducts.

Molecular Composition of the Water-Soluble Species Generated Upon Photooxidation of Maltene/Asphaltene Blends from Asphalt Binder and Coal Tar Sealant. Previous studies have demonstrated that fossil fuel-derived materials readily produce water-soluble photoproducts, with the TOC content increasing as a function of the irradiation period.[5,16,27,72] Here, we analyze the water-soluble photoproducts from the blends to determine potential correlations between maltene/asphaltene content and organic carbon production, the results for which can be seen in Figure 3.

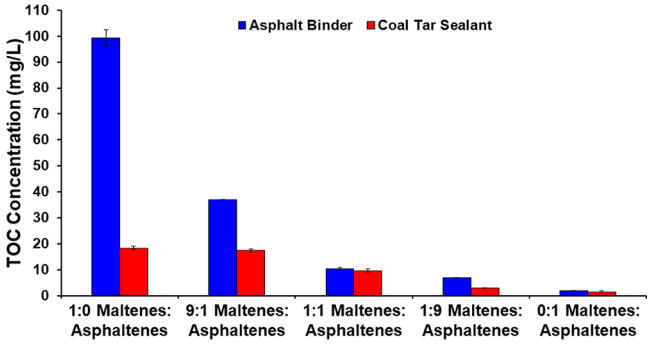

Figure 3. TOC measurements for water collected after the 48 h irradiations from the maltene and asphaltene blends from asphalt binder (blue) and coal tar sealant (red).

Overall, the petroleum-derived asphalt binder produced much higher concentrations of TOC (up to ∼99.3 mg/L) than the coal tar-based sealant (up to ∼18.3 mg/L), consistent with the previous studies that revealed that petroleum-derived materials readily leach water-soluble organic carbon upon photoirradiation.[5,27] For both the asphalt binder and coal tar sealant, the water-soluble fractions from the 1:0 maltene/asphaltene (maltene only) blend were measured at the highest TOC concentrations; asphalt binder produced ∼99.3 mg/L and coal tar sealant produced ∼18.3 mg/L. The amount of leached TOC decreased as a function of decreasing maltene content in the blends. The 0:1 maltene/asphaltene (asphaltene only) blends featured the lowest TOC values (∼2.0 and ∼1.3 mg/L). Thus, the results indicate that the maltene solubility fraction is primarily responsible for the production of water-soluble organic carbon during weathering processes. Specifically, oxygen atoms are readily incorporated into maltenic compounds through photooxidation. Note that maltenes are initially abundant in nonpolar HC species, as shown in Figure 1. Photooxidation promotes the incorporation of oxygen atoms into maltenic hydrocarbons, thereby increasing their solubility in water. In contrast, weathering of asphaltene-dominant blends results in the production of little to no water-soluble organic carbon. This trend of TOC production could potentially be attributed to the aggregation (self-association) behavior of asphaltenes. The ability of asphaltenes to self-aggregate could potentially prevent the asphaltenes from leaching organic carbon into water when exposed to solar irradiation.[68,73] Moreover, a previous report demonstrated the sample-dependent production of water-soluble species from asphaltenes. Abundant water-soluble species were observed from the irradiation of Athabasca bitumen asphaltenes.

https://doi.org/10.1021/acs.energyfuels.2c02936
Energy Fuels XXXX, XXX, XXX−XXX

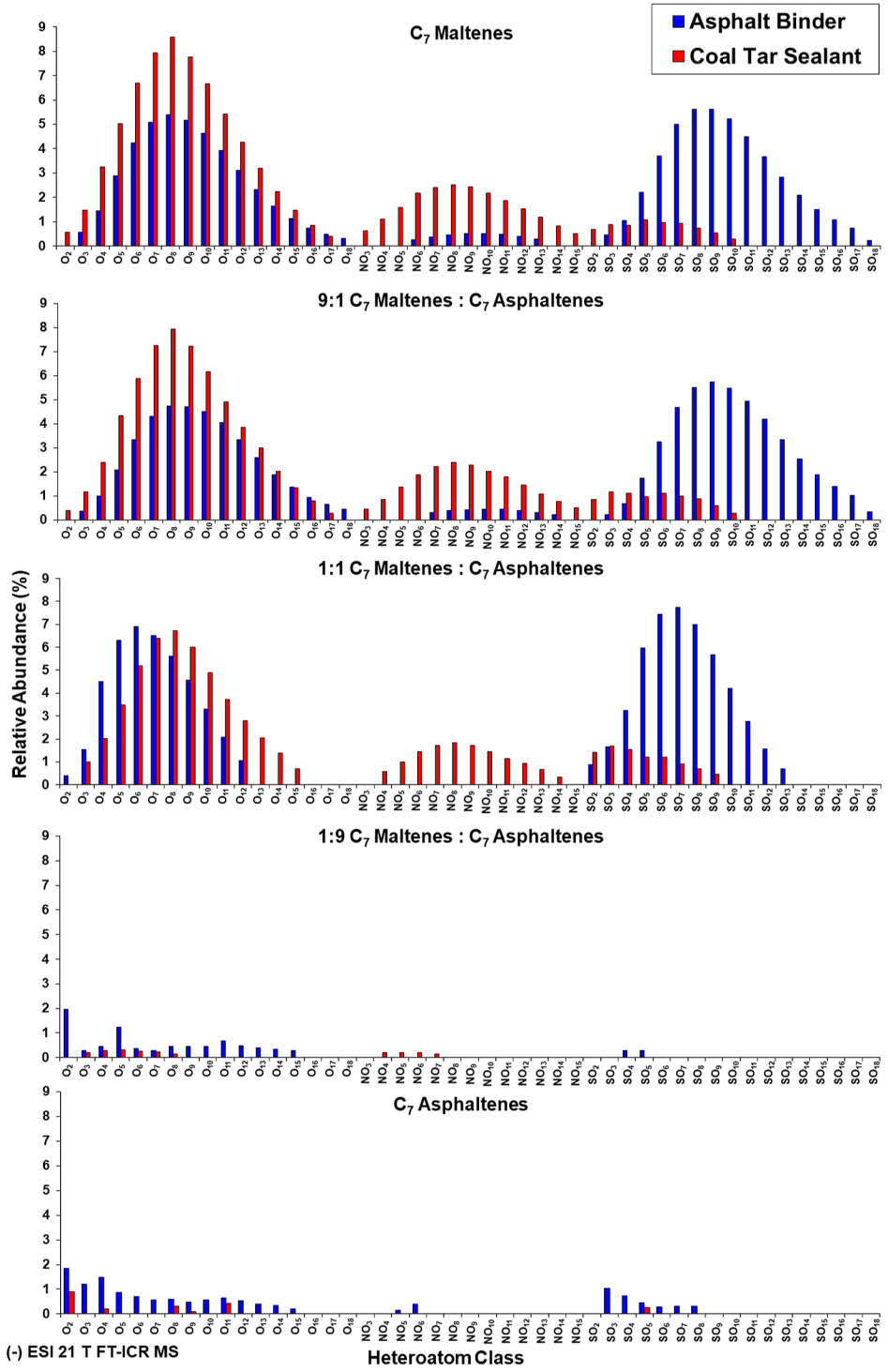

Figure 4. Heteroatom class distributions derived from (−) ESI 21 T FT-ICR MS analysis of water-soluble species generated from various maltene and asphaltene blends from asphalt binder (blue) and coal tar sealant (red).

Conversely, the irradiation of Wyoming deposit asphaltenes produced little to no water-soluble compounds, suggesting that the leachability of asphaltenes into water is sample-dependent. We hypothesize that the ability to produce water-soluble compounds could be attributed to the origin and production methods of petroleum samples.[11] For example, Athabasca bitumen is extracted from bitumen sands via a water-based method, which could potentially impact the chemistry (hydrophilicity) of the produced oil.[74]

Heteroatom Content of Water-Soluble Photoproducts. Water-soluble species produced from the irradiation of the maltene and asphaltene blends were analyzed by (−) ESI FT-ICR MS to access the polar/acidic photoproducts.[57,75−77] Figure 4 displays the relative abundances for the O_x, NO_x, and SO_x heteroatom classes detected in the water-soluble photoproducts for the five blends. It is important to note that not all of the assigned heteroatom classes are depicted in Figure 4. The heteroatom classes relevant to the results and trends discussed (highly oxidized O_x, NO_x, and SO_x) are included.

https://doi.org/10.1021/acs.energyfuels.2c02936
Energy Fuels XXXX, XXX, XXX−XXX

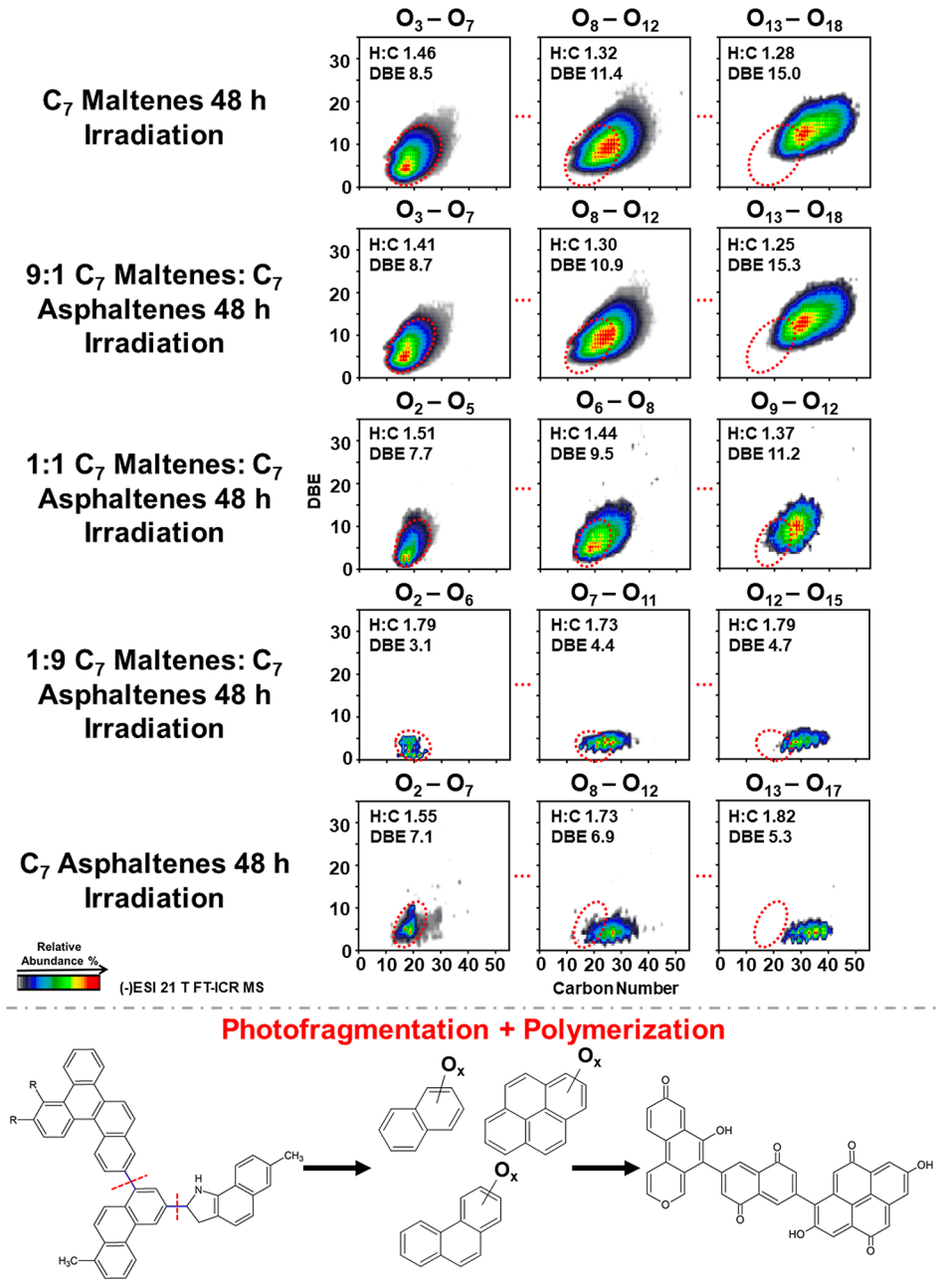

Figure 5. Isoabundance color-contoured plots of DBE vs carbon number spanning the oxygen classes contained in the water-soluble species generated from the asphalt binder maltene and asphaltene blends derived from (−) ESI 21 T FT-ICR MS analysis (top panel). Red dashed circles highlight the compositional range of the heteroatom classes with low oxygen content. Proposed pathway of formation for asphalt binder water-soluble species (bottom panel). Bonds highlighted in blue are represented as single bonds but can potentially exist as an aryl linkage, linear alkyl chains, or cycloalkyl moieties of an unknown number of carbon atoms.

For both materials, similar trends in heteroatom content are noted for the C_7 maltenes (100 wt %) and the maltene/asphaltene blends of 9:1 and 1:1. Specifically, the asphalt binder maltenes (blue bars) contain up to O_{18}, NO_{13}, and SO_{18}; the asphalt binder blend 9:1, up to O_{18}, NO_{14}, and SO_{18}; and the 1:1 blend starts the trend of decreased levels of oxidation, with only up to O_{12} and SO_{13}, with further increases in asphaltene content. Regarding the coal tar sealant, the C_7 maltenes produce water-solubles with up to O_{17}, NO_{15}, and SO_{10} classes; the blend 9:1 yields up to O_{17}, NO_{15}, and SO_{10}. Similar to asphalt binder, the coal tar photoproduct class distribution for the water-solubles from the 1:1 blend demonstrates that the degree of photooxidation decreases as a function of decreasing maltene content: this blend produced only up to O_{15}, NO_{14}, and SO_9.

It should be noted that the heteroatom content of the water-soluble photooxidized species follows the heteroatom trends established in Figure 1. For example, Figure 1 reveals that asphalt binder maltenes and asphaltenes present high abundances of sulfur-containing molecules, and likewise, the water-soluble photoproducts reveal high abundances of SO_x classes. Alternatively, coal tar sealant solubility fractions feature low abundances of S-containing species but much higher concentration of N-containing compounds, as reflected in the respective water-soluble photoproducts. It should be noted that the two asphaltene-dominant blends [1:9 and 0:1 (C_7

https://doi.org/10.1021/acs.energyfuels.2c02936
Energy Fuels XXXX, XXX, XXX−XXX

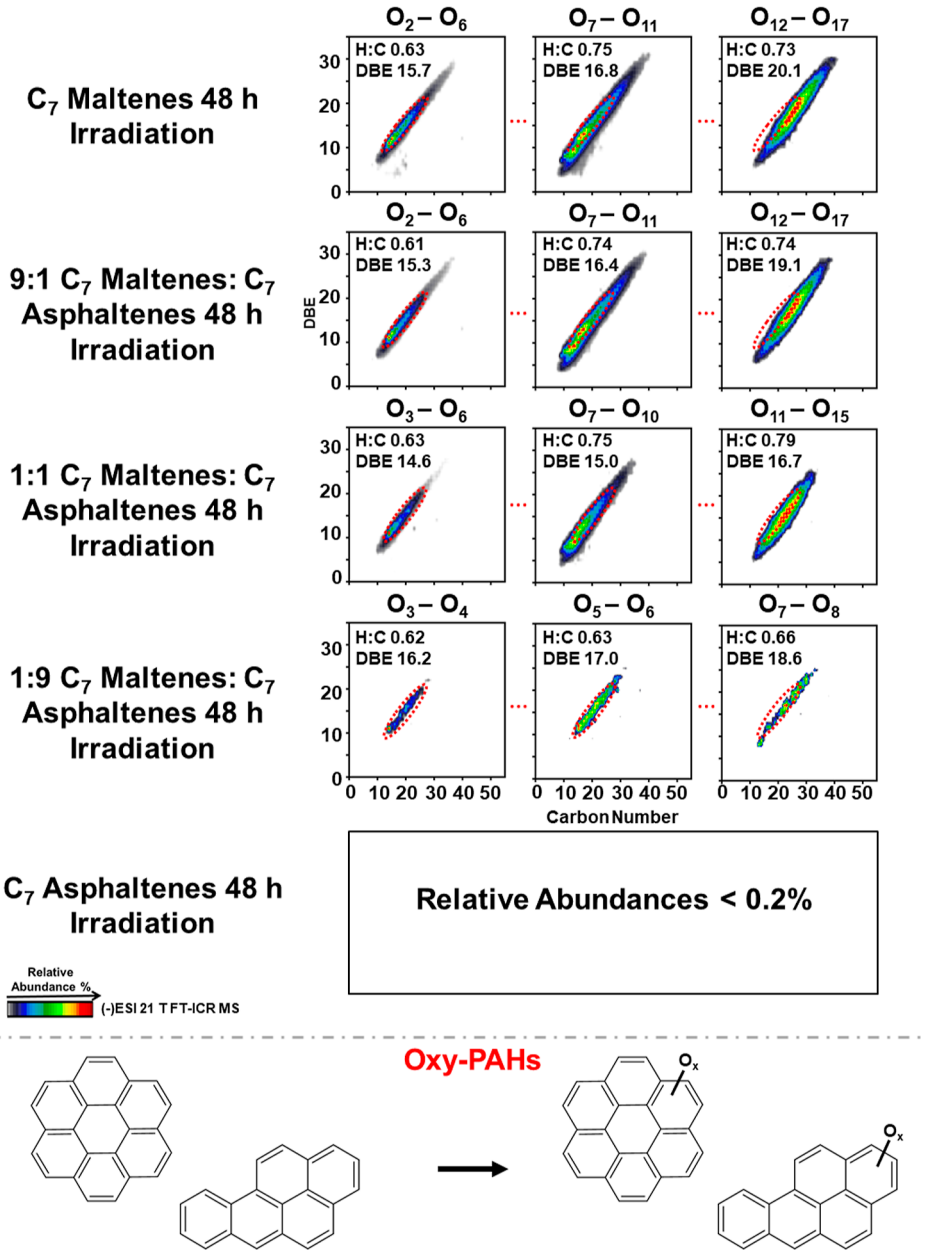

Figure 6. Isoabundance color-contoured plots of DBE vs carbon number spanning the oxygen classes contained in the water-soluble species generated from coal tar sealant maltene and asphaltene blends derived from (−) ESI 21 T FT-ICR MS analysis (top panel). Red dashed circles highlight the compositional range of the heteroatom classes with low oxygen content. Proposed pathway of formation for coal tar sealant water-soluble species (bottom panel).

asphaltenes only)] produced water-solubles in low abundance (<2% RA), and in general, asphalt binder yielded photoproducts with higher oxygen content (up to O_{15}) than that from the coal tar sealant (up to O_8). Overall, the heteroatom trends strongly suggest that C_7 maltenes play a central role in the production of oxidized water-soluble photoproducts.

Several studies have been performed regarding the blending of maltenes and asphaltenes to make artificial bitumen and to optimize paving applications. For example, Hofko et al. investigated the behavior of artificially blended bitumen at different asphaltene concentrations to determine if the blends behave like bitumen-derived materials in terms of rheological properties.[40] The authors found that the addition of asphaltenes caused a shift in the morphological structure, from a continuous "matrix" to a more polydisperse phase. Thus, the maltenes are thought to form a continuous phase with the asphaltenes, in which alkane insolubles (asphaltenes) are "dispersed". This idea, along with the fact that asphaltenes feature an intrinsic tendency to self-aggregate and form supramolecular networks,[52,55,78] which can protect asphaltenic compounds from photooxidation and even thermal cracking/hydroconversion,[68] suggests that the blending of asphaltenes with maltenes makes them more readily available to photooxidation.[79,80] These findings are in agreement with the results in Figure 4, in which photooxidation of the 9:1 and 1:1 blends, for both asphalt binder and coal tar sealant, resulted in the production of highly oxidized water-soluble species. The previous work by Chacón-Patiño et al. could shed some light on the reasons behind the production of water-solubles from asphalt binder native asphaltenes. In that report, multicore

https://doi.org/10.1021/acs.energyfuels.2c02936
Energy Fuels XXXX, XXX, XXX−XXX

enriched asphaltenes produced abundant water-soluble species, similar to the results noted for the asphalt binder (Figure 5).[11] Conversely, single-core enriched asphaltenes produced little to no water-solubles, similar to coal tar sealant results. Moreover, the trends observed for the coal tar sealant suggest that the lack of alkyl-substituents in the maltene/asphaltene molecules could also contribute to the low levels of primary water-soluble photoproducts, resulting in lower rates of secondary photooxidation.[81] One such pathway could include the primary photooxidation of benzylic carbons, which generates reactive species that subsequently photooxidize highly aromatic/alkyl-depleted species or bare PAHs.[82]

Compositional Range for Water-Soluble Species Derived from Asphalt Binder and Coal Tar Blends. The water-soluble photoproducts from the asphalt binder and the coal tar sealant blends occupy different compositional ranges, as shown in Figures 5 and 6. The compositional information is presented in combined DBE versus carbon number plots for classes with low (O_3–O_7), moderate (O_8–O_{12}), and high (O_{13}–O_{17}) oxygen content. For the three asphalt binder blends that produced abundant water-soluble species, the water-soluble photoproducts with a low content of oxygen atoms (<5) reveal DBE values between DBE 1 and 12 and carbon numbers from 10 to 30. The compositional range "shifts" to higher DBEs (up to ∼23) and carbon numbers (up to ∼50) as a function of increasing oxygen content (i.e., O_{13}–O_{18} classes). The shift to higher DBE with a concurrent increase in the carbon number, upon the addition of more oxygen atoms, has been reported for a variety of samples such as crude oil and whole asphalt binder[5,11] and suggests two possible photooxidation pathways for forming such highly oxidized water-soluble photoproducts. One possible pathway involves the presence of alkyl-substituted, high-ring-number aromatic cores in the starting material, such as ethyl coronene. High-ring-number species can incorporate more oxygen atoms than lower molecular weight aromatic cores (e.g., ethyl naphthalene), producing water-soluble/high-DBE species with a higher number of oxygen atoms.[44,83] Another possibility is the concurrent fragmentation and oxidation of multicore species to produce low-DBE oxidized "reactive" compounds that can subsequently undergo addition reactions (polymerization) to produce heavily oxidized species with higher DBE values and carbon numbers, as shown in the bottom panel of Figure 5.[5,11] It is important to note that the bridges between aromatic cores within multicore structures are represented as single bonds in Figure 5; however, the nature of these bridges is a topic of discussion, and they have been suggested to exist as an aryl linkage, linear alkyl chains, or cycloalkyl moieties of an unknown number of carbon atoms.[25]

Figure 6 presents coal tar sealant water-soluble compositions that lie along the PAH limit line, with DBE values up to ∼25 for low oxygen classes (O_2 to O_6 classes). The compositions extend to DBE 30 for heavily oxidized compounds (O_{17} class). It is important to highlight that the water-soluble photoproducts from irradiated coal tar maltenes reveal a ∼1.3-fold increase in the abundance weighted DBE as a function of the increase in the number of oxygen atoms (i.e., from O_2 to O_{17}). Conversely, the products from the irradiated asphalt binder maltenes reveal a ∼1.8-fold increase in the DBE and a ∼1.9-fold increase in the carbon number. These more pronounced changes for asphalt binder photoproducts suggest the occurrence of polymerization reactions during the photoirradiation of asphalt binder. Moreover, compositions of water-soluble species from both asphalt binder and coal tar sealant indicate that changes in the DBE and carbon number, as a function of the increasing number of oxygen atoms, become less pronounced as maltene content decreases.

It is important to highlight that coal tar sealant water-solubles reveal a compositional range highly similar to that of the starting material as they remain close to the PAH limit with narrow distributions of carbon number (Figure 6) and maintain an almost identical DBE range. Thus, when oxygen atoms are sequentially added, the change in the DBE and carbon number is not pronounced (highlighted by the red circle in Figure 6), unlike the asphalt binder, suggesting a photooxidation pathway other than polymerization. It is likely that coal tar sealant photoproducts are formed by the photooxidation of parent PAHs (with little to no alkyl substitution) with a wide range of ring numbers (e.g., anthracene and coronene). We hypothesize that these species are easily transferred to the aqueous phase with the aid of the emulsifying agent, which is present in the formulation of the coal tar sealant. Such an emulsifying additive is included in all commercially available sealants to facilitate its uniform application to paved roads and parking lots and keeps the PAHs solvated in water.[27,84] The PAHs in water can then be photooxidized to form water-soluble oxy-PAHs, with high oxygen content, that are detected in the water after solar irradiation. The contribution to the formation of water-soluble photoproducts from other additives (sand, clay, etc.) included in paving materials is the subject of future work. The slight increase in DBE as a function of the increasing number of oxygen atoms could result from the photochemical incorporation of carbonylic functionalities such as ketones, aldehydes, and carboxylic acids. The structural features of the water-soluble photoproducts will be studied in a future work by MS/MS.

Overall, the TOC measurements and the MS compositional results suggest that maltenes are pivotal in the production of water-soluble species from fossil fuel paving materials. As mentioned earlier, this result could be due to the different phases in which maltenes and asphaltenes exist. Maltenes, which exhibit a continuous phase, can be readily accessed by photooxidation, which yields abundant, oxidized photoproducts. Thus, the solubility of maltenic species in water increases. Conversely, maltene-depleted blends contain asphaltenes in a highly aggregated state. Therefore, asphaltenes present fewer species available for photooxidation, and thus, their oxygen content is not substantially altered to become water-soluble.

■ CONCLUSIONS AND FUTURE DIRECTIONS

This work sought to compare the production of water-soluble photoproducts from conventional solubility fractions, maltenes and asphaltenes, of two compositionally different road paving materials: asphalt binder and coal tar sealant. The results suggest that maltenes are central in the production of water-soluble compounds; however, asphaltenes may contribute to the production of water-soluble species depending on their concentration, aggregation state, and structural features (single-core vs multicore). Moreover, the differences in compositional trends suggest that asphalt binder and coal tar sealant produce water-soluble contaminants through different photochemical pathways, which will likely result in water-soluble compounds that have different structural characteristics. Thus, this work proposes two different photochemical

https://doi.org/10.1021/acs.energyfuels.2c02936
Energy Fuels XXXX, XXX, XXX−XXX

pathways to produce water-soluble molecules: (1) photofragmentation followed by photopolymerization and (2) photooxidation of single-core PAHs. The investigation of these two suggested pathways and the structures of the newly formed water-soluble contaminants from road paving materials will be the subject of future work.

■ ASSOCIATED CONTENT

Supporting Information

The Supporting Information is available free of charge at https://pubs.acs.org/doi/10.1021/acs.energyfuels.2c02936.

Schematic diagram of the experimental workflow; the irradiation method; recovered weight percentages after PPA precipitation; heteroatom class distributions for asphalt binder and coal tar sealant oil-soluble maltene and photoproduced asphaltene photoproducts; and isoabundance color-contoured plots of DBE versus carbon number for (+) APPI FT-ICR MS analysis of the irradiated oil-soluble photoproducts for the asphalt binder and coal tar sealant blends (PDF)

■ AUTHOR INFORMATION

Corresponding Authors

Martha L. Chacón-Patiño − *Ion Cyclotron Resonance Program, National High Magnetic Field Laboratory, Florida State University, Tallahassee, Florida 32310, United States;* orcid.org/0000-0002-7273-5343; Phone: +1 850-644-1319; Email: chacon@magnet.fsu.edu; Fax: +1 850-644-1366

Alan G. Marshall − *Ion Cyclotron Resonance Program, National High Magnetic Field Laboratory, Florida State University, Tallahassee, Florida 32310, United States; Department of Chemistry and Biochemistry, Florida State University, Tallahassee, Florida 32308, United States;* orcid.org/0000-0001-9375-2532; Phone: +1 850-644-0529; Email: marshall@magnet.fsu.edu; Fax: +1 850-644-1366

Authors

Taylor J. Glattke − *Ion Cyclotron Resonance Program, National High Magnetic Field Laboratory, Florida State University, Tallahassee, Florida 32310, United States; Department of Chemistry and Biochemistry, Florida State University, Tallahassee, Florida 32308, United States;* orcid.org/0000-0003-2934-0749

Ryan P. Rodgers − *Ion Cyclotron Resonance Program, National High Magnetic Field Laboratory, Florida State University, Tallahassee, Florida 32310, United States; Department of Chemistry and Biochemistry, Florida State University, Tallahassee, Florida 32308, United States;* orcid.org/0000-0003-1302-2850

Complete contact information is available at: https://pubs.acs.org/10.1021/acs.energyfuels.2c02936

Notes

The authors declare no competing financial interest.

■ ACKNOWLEDGMENTS

A portion of this work was performed at the National High Magnetic Field Laboratory ICR User Facility, which is supported by the National Science Foundation Division of Chemistry through cooperative agreement no. DMR-1644779 and the State of Florida.

■ REFERENCES

(1) Vaughan, P. P.; Wilson, T.; Kamerman, R.; Hagy, M. E.; McKenna, A.; Chen, H.; Jeffrey, W. H. Photochemical Changes in Water Accommodated Fractions of MC252 and Surrogate Oil Created during Solar Exposure as Determined by FT-ICR MS. *Mar. Pollut. Bull.* **2016**, *104*, 262−268.

(2) Ray, P. Z.; Chen, H.; Podgorski, D. C.; McKenna, A. M.; Tarr, M. A. Sunlight Creates Oxygenated Species in Water-Soluble Fractions of Deepwater Horizon Oil. *J. Hazard. Mater.* **2014**, *280*, 636−643.

(3) Ward, C. P.; Sharpless, C. M.; Valentine, D. L.; French-McCay, D. P.; Aeppli, C.; White, H. K.; Rodgers, R. P.; Gosselin, K. M.; Nelson, R. K.; Reddy, C. M. Partial Photochemical Oxidation Was a Dominant Fate of Deepwater Horizon Surface Oil. *Environ. Sci. Technol.* **2018**, *52*, 1797−1805.

(4) Aeppli, C.; Swarthout, R. F.; O'Neil, G. W.; Katz, S. D.; Nabi, D.; Ward, C. P.; Nelson, R. K.; Sharpless, C. M.; Reddy, C. M. How Persistent and Bioavailable Are Oxygenated Deepwater Horizon Oil Transformation Products? *Environ. Sci. Technol.* **2018**, *52*, 7250−7258.

(5) Niles, S. F.; Chacón-Patiño, M. L.; Putnam, S. P.; Rodgers, R. P.; Marshall, A. G. Characterization of Asphalt Binder and Photoproducts by FT-ICR MS Reveals Abundant Water-Soluble Hydrocarbons. *Environ. Sci. Technol.* **2020**, *54*, 8830−8836.

(6) Zito, P.; Podgorski, D. C.; Bartges, T.; Guillemette, F.; Roebuck, J. A.; Spencer, R. G. M.; Rodgers, R. P.; Tarr, M. A. Sunlight-Induced Molecular Progression of Oil into Oxidized Oil Soluble Species, Interfacial Material, and Dissolved Organic Matter. *Energy Fuels* **2020**, *34*, 4721−4726.

(7) Zhou, Z.; Liu, Z.; Guo, L. Chemical Evolution of Macondo Crude Oil during Laboratory Degradation as Characterized by Fluorescence EEMs and Hydrocarbon Composition. *Mar. Pollut. Bull.* **2013**, *66*, 164−175.

(8) Zhou, Z.; Guo, L.; Shiller, A. M.; Lohrenz, S. E.; Asper, V. L.; Osburn, C. L. Characterization of Oil Components from the Deepwater Horizon Oil Spill in the Gulf of Mexico Using Fluorescence EEM and PARAFAC Techniques. *Mar. Chem.* **2013**, *148*, 10−21.

(9) Harriman, B. H.; Zito, P.; Podgorski, D. C.; Tarr, M. A.; Suflita, J. M. Impact of Photooxidation and Biodegradation on the Fate of Oil Spilled during the Deepwater Horizon Incident: Advanced Stages of Weathering. *Environ. Sci. Technol.* **2017**, *51*, 7412−7421.

(10) Bianchi, T. S.; Osburn, C.; Shields, M. R.; Yvon-Lewis, S.; Young, J.; Guo, L.; Zhou, Z. Deepwater Horizon Oil in Gulf of Mexico Waters after 2 Years: Transformation into the Dissolved Organic Matter Pool. *Environ. Sci. Technol.* **2014**, *48*, 9288−9297.

(11) Chacón-Patiño, M. L.; Niles, S. F.; Marshall, A. G.; Hendrickson, C. L.; Rodgers, R. P. Role of Molecular Structure in the Production of Water-Soluble Species by Photooxidation of Petroleum. *Environ. Sci. Technol.* **2020**, *54*, 9968−9979.

(12) Zito, P.; Podgorski, D. C.; Bartges, T.; Guillemette, F.; Roebuck, J. A.; Spencer, R. G. M.; Rodgers, R. P.; Tarr, M. A. Sunlight-Induced Molecular Progression of Oil into Oxidized Oil Soluble Species, Interfacial Material, and Dissolved Organic Matter. *Energy Fuels* **2020**, *34*, 4721−4726.

(13) Charrié-Duhaut, A.; Lemoine, S.; Adam, P.; Connan, J.; Albrecht, P. Abiotic Oxidation of Petroleum Bitumens under Natural Conditions. *Org. Geochem.* **2000**, *31*, 977−1003.

(14) Maki, H.; Sasaki, T.; Harayama, S. Photo-Oxidation of Biodegraded Crude Oil and Toxicity of the Photo-Oxidized Products. *Chemosphere* **2001**, *44*, 1145−1151.

(15) Aeppli, C.; Carmichael, C. A.; Nelson, R. K.; Lemkau, K. L.; Graham, W. M.; Redmond, M. C.; Valentine, D. L.; Reddy, C. M. Oil Weathering after the Deepwater Horizon Disaster Led to the Formation of Oxygenated Residues. *Environ. Sci. Technol.* **2012**, *46*, 8799−8807.

(16) Chen, H.; McKenna, A. M.; Niles, S. F.; Frye, J. W.; Glattke, T. J.; Rodgers, R. P. Time-Dependent Molecular Progression and Acute Toxicity of Oil-Soluble, Interfacially-Active, and Water-Soluble Species Reveals Their Rapid Formation in the Photodegradation of Macondo Well Oil. *Sci. Total Environ.* **2022**, *813*, 151884.
(17) Speight, J. G. Asphalt Paving. *Asphalt Materials Science and Technology*; Butterworth-Heinemann, 2016; pp 409−435.
(18) De Brimont, M. R.; Hörnig, A.; Jensen, E. S.; Olsen, J. E. Lightweight Filler for Waterproofing Bitumen Membranes. U.S. Patent 20,190,255,810 A1, 2019.
(19) Smith, J. D.; Mellott, I. J. W.; Rus, M.; Sokol, D.; Holland, J. Active Polymer Modification of Bitumen for Use in Roofing Materials. U.S. Patent 9,745,473 B2, 2017.
(20) Rahman, M. T.; Mohajerani, A.; Giustozzi, F. Recycling of Waste Materials for Asphalt Concrete and Bitumen: A Review. *Materials* **2020**, *13*, 1495.
(21) Yuan, G.; Xue, Z.; Cui, Z.; Westwood, A.; Dong, Z.; Cong, Y.; Zhang, J.; Zhu, H.; Li, X. Constructing the Bridge from Isotropic to Anisotropic Pitches for Preparing Pitch-Based Carbon Fibers with Tunable Structures and Properties. *ACS Omega* **2020**, *5*, 21948−21960.
(22) Bowman, D. T.; Jobst, K. J.; Helm, P. A.; Kleywegt, S.; Diamond, M. L. Characterization of Polycyclic Aromatic Compounds in Commercial Pavement Sealcoat Products for Enhanced Source Apportionment. *Environ. Sci. Technol.* **2019**, *53*, 3157−3165.
(23) Giger, W.; Blumer, M. Polycyclic Aromatic Hydrocarbons in the Environment. Isolation and Characterization by Chromatography, Visible, Ultraviolet, and Mass Spectrometry. *Anal. Chem.* **1974**, *46*, 1663−1671.
(24) Magi, E.; Di Carro, M. Marine Environment Pollution: The Contribution of Mass Spectrometry to the Study of Seawater. *Mass Spectrom. Rev.* **2018**, *37*, 492−512.
(25) Chacón-Patiño, M. L.; Gray, M. R.; Rüger, C.; Smith, D. F.; Glattke, T. J.; Niles, S. F.; Neumann, A.; Weisbrod, C. R.; Yen, A.; McKenna, A. M.; Giusti, P.; Bouyssiere, B.; Barrère-Mangote, C.; Yarranton, H.; Hendrickson, C. L.; Marshall, A. G.; Rodgers, R. P. Lessons Learned from a Decade-Long Assessment of Asphaltenes by Ultrahigh-Resolution Mass Spectrometry and Implications for Complex Mixture Analysis. *Energy Fuels* **2021**, *35*, 16335−16376.
(26) Niles, S. F.; Chacón-Patiño, M. L.; Chen, H.; McKenna, A. M.; Blakney, G. T.; Rodgers, R. P.; Marshall, A. G. Molecular-Level Characterization of Oil-Soluble Ketone/Aldehyde Photo-Oxidation Products by Fourier Transform Ion Cyclotron Resonance Mass Spectrometry Reveals Similarity between Microcosm and Field Samples. *Environ. Sci. Technol.* **2019**, *53*, 6887−6894.
(27) Glattke, T. J.; Chacón-Patiño, M. L.; Hoque, S. S.; Ennis, T. E.; Greason, S.; Marshall, R. P.; Rodgers, A. G. Complex Mixture Analysis of Emerging Contaminants Generated from Coal Tar- and Petroleum-Derived Pavement Sealants: Molecular Compositions and Correlations with Toxicity Revealed by Fourier Transform Ion Cyclotron Resonance Mass Spectrometry. *Environ. Sci. Technol.* **2022**, *56*, 12988−12998.
(28) Mahler, B. J.; Metre, P. C.; Crane, J. L.; Watts, A. W.; Scoggins, M.; Williams, E. S. Coal-Tar-Based Pavement Sealcoat and PAHs: Implications for the Environment, Human Health, and Stormwater Management. *Environ. Sci. Technol.* **2012**, *46*, 3039−3045.
(29) Mahler, B. J.; Van Metre, P. C.; Bashara, T. J.; Wilson, J. T.; Johns, D. A. Parking Lot Sealcoat: An Unrecognized Source of Urban Polycyclic Aromatic Hydrocarbons. *Environ. Sci. Technol.* **2005**, *39*, 5560−5566.
(30) Van Metre, P. C.; Mahler, B. J. PAH Concentrations in Lake Sediment Decline Following Ban on Coal-Tar-Based Pavement Sealants in Austin, Texas. *Environ. Sci. Technol.* **2014**, *48*, 7222−7228.
(31) Actions to restrict or discontinue the use of Coal Tar Based Sealants in the United States. https://www.pca.state.mn.us/sites/default/files/tdr-g1-12.pdf (accessed May 10, 2021).
(32) McClintock, N.; Turner, M.; Gosselink, L.; Scoggins, M. *PAHs in Austin, Texas Sediments and Coal-Tar Based Pavement Sealants Polycyclic Aromatic Hydrocarbons*; Texas Watershed Protection and Development Review Department: Austin, 2005.
(33) Crane, J.; Grosenheider, K.; Wilson, C. B. *Contamination of Stormwater Pond Sediments by Polycyclic Aromatic Hydrocarbons (PAHs) in Minnesota*; Minnesota Pollution Control Agency: St. Paul, 2010.
(34) Hsu, C. S.; Lobodin, V. V.; Rodgers, R. P.; McKenna, A. M.; Marshall, A. G. Compositional Boundaries for Fossil Hydrocarbons. *Energy Fuels* **2011**, *25*, 2174−2178.
(35) Chacón-Patiño, M. L.; Blanco-Tirado, C.; Orrego-Ruiz, J. A.; Gómez-Escudero, A.; Combariza, M. Y. Tracing the Compositional Changes of Asphaltenes after Hydroconversion and Thermal Cracking Processes by High-Resolution Mass Spectrometry. *Energy Fuels* **2015**, *29*, 6330−6341.
(36) McKenna, A. M.; Marshall, A. G.; Rodgers, R. P. Heavy Petroleum Composition. 4. Asphaltene Compositional Space. *Energy Fuels* **2013**, *27*, 1257−1267.
(37) Zheng, F.; Shi, Q.; Vallverdu, G. S.; Giusti, P.; Bouyssiere, B. Fractionation and Characterization of Petroleum Asphaltene: Focus on Metalopetroleomics. *Processes* **2020**, *8*, 1504.
(38) Fakher, S.; Ahdaya, M.; Elturki, M.; Imqam, A. Critical Review of Asphaltene Properties and Factors Impacting Its Stability in Crude Oil. *J. Pet. Explor. Prod. Technol.* **2020**, *10*, 1183−1200.
(39) Aljaafari, Z.; Ismael, M. Q. The Influence of Chemical Composition of Asphalt Cement on the Physical and Rheological Properties. *J. Eng. Sci. Technol.* **2020**, *15*, 4303−4319.
(40) Hofko, B.; Eberhardsteiner, L.; Füssl, J.; Grothe, H.; Handle, F.; Hospodka, M.; Grossegger, D.; Nahar, S. N.; Schmets, A. J. M.; Scarpas, A. Impact of Maltene and Asphaltene Fraction on Mechanical Behavior and Microstructure of Bitumen. *Mater. Struct. Constr.* **2016**, *49*, 829−841.
(41) Li, F.; Wang, Y.; Zhao, K. Connections between Asphaltene Microstructures in Aged Asphalt Binders and Performance-Related Engineering Properties. *Constr. Build. Mater.* **2022**, *329*, 127173.
(42) Glattke, T. J.; Chacón-Patiño, M. L.; Marshall, A. G.; Rodgers, R. P. Molecular Characterization of Photochemically Produced Asphaltenes via Photooxidation of Deasphalted Crude Oils. *Energy Fuels* **2020**, *34*, 14419−14428.
(43) Pesarini, P. F.; de Souza, R. G. S.; Corrêa, R. J.; Nicodem, D. E.; de Lucas, N. C. Asphaltene Concentration and Compositional Alterations upon Solar Irradiation of Petroleum. *J. Photochem. Photobiol., A* **2010**, *214*, 48−53.
(44) Cope, V. W.; Kalkwarf, D. R. Photooxidation of Selected Polycyclic Aromatic Hydrocarbons and Pyrenequinones Coated on Glass Surfaces. *Environ. Sci. Technol.* **1987**, *21*, 643−648.
(45) Lesueur, D. The Colloidal Structure of Bitumen: Consequences on the Rheology and on the Mechanisms of Bitumen Modification. *Adv. Colloid Interface Sci.* **2009**, *145*, 42−82.
(46) Chacón-Patiño, M. L.; Rowland, S. M.; Rodgers, R. P. Advances in Asphaltene Petroleomics. Part 3. Dominance of Island or Archipelago Structural Motif Is Sample Dependent. *Energy Fuels* **2018**, *32*, 9106−9120.
(47) Morgan, T. J.; Alvarez-Rodriguez, P.; George, A.; Herod, A. A.; Kandiyoti, R. Characterization of Maya Crude Oil Maltenes and Asphaltenes in Terms of Structural Parameters Calculated from Nuclear Magnetic Resonance (NMR) Spectroscopy and Laser Desorption-Mass Spectroscopy (LD-MS). *Energy Fuels* **2010**, *24*, 3977−3989.
(48) Boduszynski, M. M.; Hurtubise, R. J.; Silver, H. F. Separation of Solvent-Refined Coal into Compound-Class Fractions. *Anal. Chem.* **1982**, *54*, 375−381.
(49) Boduszynski, M. M. Composition of Heavy Petroleums. 2. Molecular Characterization. *Energy Fuels* **1988**, *2*, 597−613.
(50) Moseley, H. L.; Page, G. C.; Musselman, J. A.; Sholar, G. A.; Upshaw, P. B. *Laboratory Mixture and Binder Rutting Study*, 2003.
(51) U.S. EPA. *Method 8270E (SW-846): Semivolatile Organic Compounds by Gas Chromatography/Mass Spectrometry (GC/MS)*, Washington DC, 2014.

https://doi.org/10.1021/acs.energyfuels.2c02936
Energy Fuels XXXX, XXX, XXX−XXX

(52) Chacón-Patiño, M. L.; Rowland, S. M.; Rodgers, R. P. Advances in Asphaltene Petroleomics. Part 2: Selective Separation Method That Reveals Fractions Enriched in Island and Archipelago Structural Motifs by Mass Spectrometry. *Energy Fuels* **2018**, *32*, 314−328.
(53) King, S. M.; Leaf, P. A.; Olson, A. C.; Zito, P. Z.; Tarr, M. A. Photolytic and Photocatalytic Degradation of Surface Oil from the Deepwater Horizon Spill. *Chemosphere* **2014**, *95*, 415−422.
(54) Lipps, W. C.; Baxter, T. E.; Braun-Howland, E. 5310 Total Organic Carbon. In *Standard Methods for the Examination of Water and Wastewater*; APHA Press: Washington DC, 2018.
(55) Gray, M. R.; Tykwinski, R. R.; Stryker, J. M.; Tan, X. Supramolecular Assembly Model for Aggregation of Petroleum Asphaltenes. *Energy Fuels* **2011**, *25*, 3125−3134.
(56) Smith, D. F.; Podgorski, D. C.; Rodgers, R. P.; Blakney, G. T.; Hendrickson, C. L. 21 Tesla FT-ICR Mass Spectrometer for Ultrahigh-Resolution Analysis of Complex Organic Mixtures. *Anal. Chem.* **2018**, *90*, 2041−2047.
(57) Ruddy, B. M.; Huettel, M.; Kostka, J. E.; Lobodin, V. V.; Bythell, B. J.; McKenna, A. M.; Aeppli, C.; Reddy, C. M.; Nelson, R. K.; Marshall, A. G.; Rodgers, R. P. Targeted Petroleomics: Analytical Investigation of Macondo Well Oil Oxidation Products from Pensacola Beach. *Energy Fuels* **2014**, *28*, 4043−4050.
(58) Kaiser, N. K.; Savory, J. J.; Hendrickson, C. L. Controlled Ion Ejection from an External Trap for Extended m/z Range in FT-ICR Mass Spectrometry. *J. Am. Soc. Mass Spectrom.* **2014**, *25*, 943−949.
(59) Blakney, G. T.; Hendrickson, C. L.; Marshall, A. G. Predator Data Station: A Fast Data Acquisition System for Advanced FT-ICR MS Experiments. *Int. J. Mass Spectrom.* **2011**, *306*, 246−252.
(60) Chacón-Patiño, M. L.; Moulian, R.; Barrère-Mangote, C.; Putman, J. C.; Weisbrod, C. R.; Blakney, G. T.; Bouyssiere, B.; Rodgers, R. P.; Giusti, P. Compositional Trends for Total Vanadium Content and Vanadyl Porphyrins in Gel Permeation Chromatography Fractions Reveal Correlations between Asphaltene Aggregation and Ion Production Efficiency in Atmospheric Pressure Photoionization. *Energy Fuels* **2020**, *34*, 16158−16172.
(61) Xian, F.; Hendrickson, C. L.; Blakney, G. T.; Beu, S. C.; Marshall, A. G. Automated Broadband Phase Correction of Fourier Transform Ion Cyclotron Resonance Mass Spectra. *Anal. Chem.* **2010**, *82*, 8807−8812.
(62) Corilo, Y. E. *PetroOrg Software*; Florida State Univsersity, 2013.
(63) Rodgers, R. P.; Marshall, A. G. Petroleomics: Advanced Characterization of Petroleum Derived Materials by Fourier Transform Ion Cyclotron Resonance Mass Spectrometry (FTICR MS). In *Asphaltenes, Heavy Oils, and Petroleomics*; Springer: New York, NY, 2007; pp 63−93.
(64) Punase, A.; Prakoso, A.; Hascakir, B. The Polarity of Crude Oil Fractions Affects the Asphaltenes Stability. *Society of Petroleum Engineers—SPE Western Regional Meeting*, 2016.
(65) Mullins, O. C. The Asphaltenes. *Annu. Rev. Anal. Chem.* **2011**, *4*, 393−418.
(66) Mullins, O. C.; Sabbah, H.; Eyssautier, J.; Pomerantz, A. E.; Barré, L.; Andrews, A. B.; Ruiz-Morales, Y.; Mostowfi, F.; McFarlane, R.; Goual, L.; Lepkowicz, R.; Cooper, T.; Orbulescu, J.; Leblanc, R. M.; Edwards, J.; Zare, R. N. Advances in Asphaltene Science and the Yen-Mullins Model. *Energy Fuels* **2012**, *26*, 3986−4003.
(67) Durand, E.; Clemancey, M.; Lancelin, J. M.; Verstraete, J.; Espinat, D.; Quoineaud, A. A. Effect of Chemical Composition on Asphaltenes Aggregation. *Energy Fuels* **2010**, *24*, 1051−1062.
(68) Chacón-Patiño, M. L.; Heshka, N.; Alvarez-Majmutov, A.; Hendrickson, C. L.; Rodgers, R. P. Molecular Characterization of Remnant Polarizable Asphaltene Fractions Upon Bitumen Upgrading and Possible Implications in Petroleum Viscosity. *Energy Fuels* **2022**, *36*, 7542−7557.
(69) Chung, S. H.; Violi, A. Peri-Condensed Aromatics with Aliphatic Chains as Key Intermediates for the Nucleation of Aromatic Hydrocarbons. *Proc. Combust. Inst.* **2011**, *33*, 693−700.
(70) Niles, S. F.; Chacón-Patiño, M. L.; Smith, D. F.; Rodgers, R. P.; Marshall, A. G. Comprehensive Compositional and Structural Comparison of Coal and Petroleum Asphaltenes Based on Extrography Fractionation Coupled with Fourier Transform Ion Cyclotron Resonance MS and MS/MS Analysis. *Energy Fuels* **2020**, *34*, 1492−1505.
(71) Chacón-Patiño, M. L.; Smith, D. F.; Hendrickson, C. L.; Marshall, A. G.; Rodgers, R. P. Advances in Asphaltene Petroleomics. Part 4. Compositional Trends of Solubility Subfractions Reveal That Polyfunctional Oxygen-Containing Compounds Drive Asphaltene Chemistry. *Energy Fuels* **2020**, *34*, 3013−3030.
(72) Niles, S. F.; Chacón-Patiño, M. L.; Chen, H.; Marshall, A. G.; Rodgers, R. P. Structural Dependence of Photogenerated Transformation Products for Aromatic Hydrocarbons Isolated from Petroleum. *Energy Fuels* **2021**, *35*, 18153−18162.
(73) Zhang, Y.; Siskin, M.; Gray, M. R.; Walters, C. C.; Rodgers, R. P. Mechanisms of Asphaltene Aggregation: Puzzles and a New Hypothesis. *Energy Fuels* **2020**, *34*, 9094−9107.
(74) Masliyah, J.; Zhou, Z.; Xu, Z.; Czarnecki, J.; Hamza, H. Understanding Water-Based Bitumen Extraction from Athabasca Oil Sands. *Can. J. Chem. Eng.* **2004**, *82*, 628−654.
(75) Kellerman, A. M.; Dittmar, T.; Kothawala, D. N.; Tranvik, L. J. Chemodiversity of Dissolved Organic Matter in Lakes Driven by Climate and Hydrology. *Nat. Commun.* **2014**, *5*, 3804.
(76) Kellerman, A. M.; Kothawala, D. N.; Dittmar, T.; Tranvik, L. J. Persistence of Dissolved Organic Matter in Lakes Related to Its Molecular Characteristics. *Nat. Geosci.* **2015**, *8*, 454−457.
(77) Xu, W.; Gao, Q.; He, C.; Shi, Q.; Hou, Z. Q.; Zhao, H. Z. Using ESI FT-ICR MS to Characterize Dissolved Organic Matter in Salt Lakes with Different Salinity. *Environ. Sci. Technol.* **2020**, *54*, 12929−12937.
(78) Chacón-Patiño, M. L.; Rowland, S. M.; Rodgers, R. P. Advances in Asphaltene Petroleomics. Part 1: Asphaltenes Are Composed of Abundant Island and Archipelago Structural Motifs. *Energy Fuels* **2017**, *31*, 13509−13518.
(79) Bearsley, S.; Forbes, A.; Haverkamp, R. G. Direct Observation of the Asphaltene Structure in Paving-Grade Bitumen Using Confocal Laser-Scanning Microscopy. *J. Microsc.* **2004**, *215*, 149−155.
(80) Gray, M. R.; Yarranton, H. W.; Chacón-Patiño, M. L.; Rodgers, R. P.; Bouyssiere, B.; Giusti, P. Distributed Properties of Asphaltene Nanoaggregates in Crude Oils: A Review. *Energy Fuels* **2021**, *35*, 18078−18103.
(81) Mallakin, A.; George Dixon, D.; Greenberg, B. M. Pathway of Anthracene Modification under Simulated Solar Radiation. *Chemosphere* **2000**, *40*, 1435−1441.
(82) Nikitas, N. F.; Tzaras, D. I.; Triandafillidi, I.; Kokotos, C. G. Photochemical Oxidation of Benzylic Primary and Secondary Alcohols Utilizing Air as the Oxidant. *Green Chem.* **2020**, *22*, 471−477.
(83) Kohtani, S.; Tomohiro, M.; Tokumura, K.; Nakagaki, R. Photooxidation Reactions of Polycyclic Aromatic Hydrocarbons over Pure and Ag-Loaded BiVO4 Photocatalysts. *Appl. Catal., B* **2005**, *58*, 265−272.
(84) Roberts, F. L.; Kandhal, P. S.; Brown, E. R.; Lee, D. Y.; Kennedy, T. W. *Hot Mix Asphalt Materials, Mixture Design, and Construction*; National Asphalt Pavement Association Education Foundation: Lanham, MD, 1996.

https://doi.org/10.1021/acs.energyfuels.2c02936
Energy Fuels XXXX, XXX, XXX−XXX